Journal of Manufacturing Engineering, September 2025, Vol. 20, Issue. 3, pp 113-121
DOI: https://doi.org/10.37255/jme.v20i3pp113-121

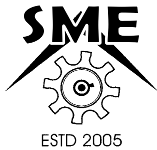

IMPACT OF METAL-WORK FUNCTION AND TEMPERATURE ON THE PERFORMANCE OF SCHOTTKY BARRIER DIODE DEVICES

Sonia Bouzgarrou

Department of Physics, College of Science, Qassim University, 51452, Buraidah, Saudi Arabia.
Laboratoire de Microélectronique et Instrumentation (UR 03/13-04), Faculté des Sciences de Monastir, Avenue de l'Environnement 5000 Monastir, Tunisia

Abstract

N-Aluminum Gallium Arsenide Schottky Diodes are studied by I-V characteristics. Current-voltage characteristics were analyzed for some Metal-Work Functions at a 300K temperature. A significant dependence was observed between this parameter and the electrical parameters. These results demonstrate that it affects the device's performance. Important electrical characteristics, like saturation current (Is), series resistances (Rs), ideality factor (n), and barrier height ($\emptyset bn$), are also defined for various temperature values by analyzing the current-voltage ($I-V$) behavior. R, Øb, and n parameters are computed using the Cheung method and the thermionic emission (TE) theory. The ideality factor (n) values were found to drop as temperatures increased, but the barrier height ($\emptyset bn$) increased. The ideality factor values at the contact interface were found to exhibit a double Gaussian distribution based on temperature-dependent observations. Comparing the results to the experimental data revealed an equal result. These findings suggest that the n-AlGaAs structure may be effectively utilized in optoelectronic and photovoltaic applications, demonstrating excellent diode properties for solar cells. As a result, the outcomes of this recent research logically support the idea that these Schottky barrier diodes are ideal for effectively harvesting renewable energy.

Keywords: *Metal-Work Functions, Schottky diode, Barrier height, Electrical behavior, Ideality factor, Metal-semiconductor contacts, thermionic emission.*

1. Introduction

The Schottky diode (SD) is a semiconductor device with a metal surface contact. F. Braun discovered the first diodes in 1874 [1]; although they are quite old, they remain a subject of research today due to their numerous applications. Recently, SD has been applied in various areas, including solar cells, microwave jammer detectors, Zener diodes, and integrated circuits. SD are widespread components in the electronics sector [2-7]. They are used in devices of all sizes, ranging from low-power units to large industrial equipment. These components belong to the category of diodes. They are electronic components that regulate the electrical flow, allowing it to pass in only one direction and preventing it from passing in the other. These diodes are specified to operate at different current and voltage levels; any use in capacities incompatible with their specifications may cause failure. SDs are also used to protect transistors through voltage blocking [8-13].

MS (Metal-Semiconductor) contact, specifically Schottky barrier diodes (SBDs), is a critical area of research [14]. This can significantly impact the performance of SD on the reliability and efficiency of various electronic devices. There are two important advantages of placing an insulating layer (MIS) between the metal and semiconductor [15]. It functions as a dielectric barrier, altering the characteristics of the Schottky barrier and potentially enhancing performance in applications such as switching and current rectification. The Schottky diode's I-V properties, such as its ideality factor, turn-on voltage, and reverse saturation current, can provide information on the strength of the MS contact and the diode's overall performance. The Schottky barrier height ($\emptyset bn$) can be considerably changed by the insulating layer. We can adjust the Schottky diode's behavior, such as lowering the forward voltage drop or enhancing the reverse leakage current characteristics, by adjusting the thickness and features of this insulating layer. For specific applications, such as high-speed switching or low-power devices, this technique is often employed to enhance the diode.

The barrier height ($\emptyset bn$) can change with the applied-bias voltage due to various factors, such as changes in contact potential at the interface. Due to this fluctuation, it may be challenging to derive a precise and

**Corresponding Author -E-mail: b_sonia3@yahoo.fr*

 © SME

consistent value for the barrier height across all voltage ranges. Temperature affects the ideality factor and the barrier height. According to certain research, such tunneling or recombination can cause the ideality factor to rise at high temperatures. On the other hand, because thermionic emission predominates at low temperatures, the diode can be used more effectively with a lower ideality factor.

This investigation examines the electrical characteristics of an n-AlGaAs Schottky diode made by the deposition process using I-V methods at room temperature for various work functions. In addition, $I - V$ modulations were performed at various temperature values to demonstrate how temperature affects structural performance and to understand the behavior of the device's barrier homogeneity. Using the numerical simulator in the MATLAB programming language, series resistance (Rs), barrier height ($\emptyset bn$), and the ideality factor (n) of n-AlGaAs SD were examined by applying two methods, classical and Cheung-Cheung methods, among other electrical properties. The impact of high temperatures on the variables of the SD is discussed in the next sections.

2. Structure and Simulation

Schottky diode-contacts AlGaAs structures with n-doping were simulated and discussed using the MATLAB programming language. The doping concentration of the epitaxial layer is 3*1016 cm-3 above the substrate GaAs and 2*1016 cm-3 doped epilayer under Schottky contact, as shown in Figure 1. The layer structure of our device consists of a 0.45 µm undoped GaAs buffer layer, followed by a 1 µm-thick AlGaAs epitaxial layer. Schottky contact with a diameter of 0.5µm on the topside of the sample, in a circular form. The effect is neglected by taking a very low density of donor and acceptor states. After defining the structure device, it considers all the optical and electrical characteristics, including the band gap (Eg), electric affinity (χ), dielectric constant (ε), effective state density of the conduction band (Nc), valence state density (Nv), electron mobility (µn), hole mobility (µp), and other electrical characteristics. Additionally, the effects of temperature and work function on the electrical behavior of the metal/n-AlGaAs Schottky structure were investigated. The Poisson equation and the continuity equation for both hole and electron carriers are the fundamental formulas of the MATLAB simulator. The space density of charges [16] and electrostatic potential have relations to the Poisson equation and are provided by:

$$div\,(grad\,\psi) = -\,\rho/\varepsilon 0 \quad (1)$$

where ψ is the electrostatic potential, ε is the permittivity, and ρ is the space charge density. The continuity equations, for electron and hole carriers, are expressed by:

$$\frac{\partial n}{\partial t} = \frac{1}{q}\ div\,J_n - R_n + G_n$$
$$\frac{\partial p}{\partial t} = \frac{1}{q}\ div\,J_p - R_p + G_p$$

where n and p, are the electron and hole concentrations, Jn and Jp are the electron and hole current densities, Gn and Gp are the generation rates for electrons and holes, Rn and Rp are the recombination rates for electrons and holes, and q is the electron charge. Physical methods such as concentration-dependent mobility (CONMOB) [17, 18], Auger recombination rate (Auger) [19], and Shockley-Read-Hall (SRH) recombination [20] are utilized. In addition, the numerical solution processes used are the classical method and the Cheung-Cheung method.

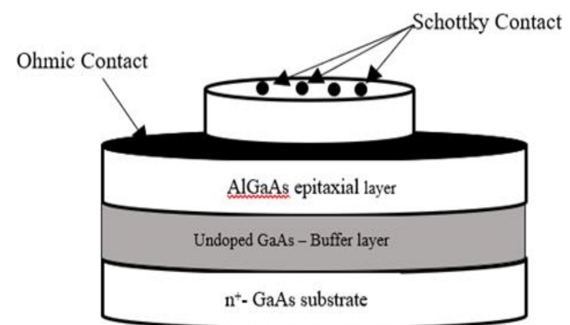

Fig. 1. Schematic of the fabricated simulated device n-AlGaAs Schottky diode structure

3. Simulation Part

3.1 Work Function dependence of $I - V$ characteristics investigated

An essential component of semiconductor technology is metal. They form ohmic contacts, Schottky barriers, and gates in field effect transistors, in addition to being employed as interconnects or low-resistance conductors. In semiconductor circuits, interconnects offer channels for charge to move between locations. Although passive components of the circuit, these interconnects are crucial and significantly impact the circuit's operation. Interconnects are placed above insulators, and they only come into contact with the active devices when specific windows are opened. Metal strips for interconnects must have sufficient current-carrying capacity and establish excellent contact with the devices. For these reasons, in this section, we consider

Journal of Manufacturing Engineering, September 2025, Vol. 20, Issue. 3, pp 113-121
DOI: https://doi.org/10.37255/jme.v20i3pp113-121

the work function values of some metals, as shown in Table 1 [21, 22].

The Metal-Work Function effect is studied at room temperature. Linear characteristics and semi-log of $(I - V)$ of metal /n-AlGaAs Schottky structure, are shown in Figure 2, for some metal work Functions. This result shows that, for all values of $\emptyset m$, Schottky characteristics exhibit behavior at forward bias voltages at low bias voltages, V > 0.75V. During this interval of low bias, the current increases linearly with the bias voltage and subsequently decreases as $\emptyset m$ increases. Nevertheless, at a high area voltage, when V < 0.75V, the series resistance effect is observed by a linearity deviation with increasing bias voltage. However, for $\emptyset m > 4.94eV$, it is clear that $I - V$ characteristics at low bias show two separate sections of lines with two different slopes. Region I is located at low bias voltages (V ≤), while Region II is located at bias voltages between 0.35V and 0.75V. Under this low forward bias, this double barrier event can be recognized as the emergence of an anomalous current [23]. In summary, the current progressively drops with rising $\emptyset m$ for linear characteristics and forward bias voltage, and it grows linearly with bias voltage. Furthermore, it is noted that when $\emptyset m$ increases, the threshold voltage VT also increases. We can conclude that the Metal-Work Function influences the device's performance.

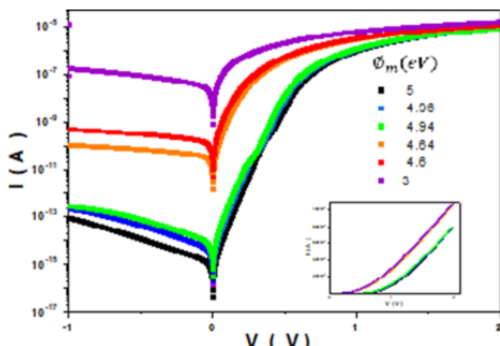

Fig. 2. Room temperature characteristics I-V of n-AlGaAs for some Metal-Work Function.

3.2 Temperature dependence of $I - V$ characteristics

I-V characteristics evaluated at a single temperature might not be enough to examine the diode's electrical properties. To better understand the current conduction mechanism in diodes, several temperature values are therefore required [25, 26]. This section focused on how temperatures modify the electrical behavior of the metal n-AlGaAs Schottky contacts for a fixed work function ∅, m = 4.96 eV. The characteristics of the forward and reverse biases of the Schottky contact on both linear and semi-logarithmic scales, simulated at temperatures ranging from 100K to 500K, are shown in Figures 3 and 4, respectively.

At low bias voltages (V > 0.75V), the current increases rapidly as the bias voltage rises, varies linearly with the bias voltage, and gradually shifts toward the higher bias side as the temperature decreases. The threshold voltage is quickly reached as the temperature increases. On the other hand, at high bias voltages (V < 0.75V), the current exhibits a significant decrease, fluctuates linearly with the bias voltage, and progressively increases as the temperature rises.

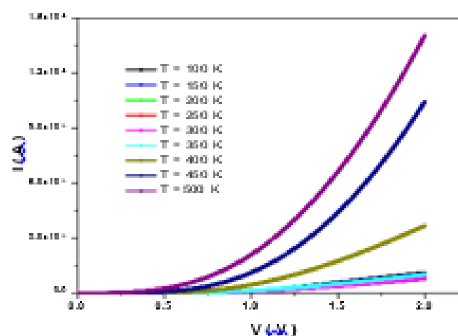

Fig. 3. forward I-V characteristics of the n-AlGaAs Schottky diode at different temperatures (100K-500K).

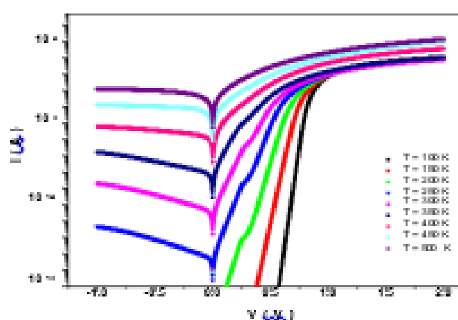

Fig. 4. Semilogarithmic I-V characteristics of n-AlGaAs SD at different temperatures (100K-500K).

As can be seen, moreover, the current is low at low temperatures due to the rise in series resistance, which is well observed. The value of the current at 100K is very small due to the freezing phenomenon, where the mobility of carriers is very low. Conversely, the current rises as the temperature rises to 500K. Therefore, due to the combined influence of temperature and barrier height on the saturation current, we observe a significant leakage current. As the reverse bias increases, the inverse current also increases; however, saturation is not observed. This is a well-known phenomenon associated with defects, such as bulk defects and surface states.

In addition, we can observe that both the forward and reverse currents increase as the temperature

rises, suggesting a typical thermal activation. We can analyze these attributes in depth by obtaining the SD parameters in the next part of our study. To extract electrical characteristics, such as ideal factor, saturation current, and high barrier, there are several methods for extracting these parameters; we will focus on the following two methods (Classical and Cheung-Cheung).

3.2.1. Classical method / thermionic emission theory

SD has been effectively described in terms of bias in accordance with the thermionic emission theory. The current and voltage relation for moderate forward bias voltages is given, as expressed as [27, 28]:

$$I = I_s \left[exp \frac{(V-R_s I)}{nV_t} - 1\right] \quad (4)$$

where, $V_t = kT/q$

$$I = I_s \left[exp \frac{q(V-R_s I)}{nkT} - 1\right] \quad (5)$$

where q is the electron charge, k is the Boltzmann constant, V is the forward-bias applied voltage, T is the temperature in kelvin, n is the ideality factor, and Rs is the series resistance.

In this equation, the reverse-saturation current at zero bias voltage is denoted by I. Which is defined as the following equation:

$$I_s = AA^*T^2 exp\left(\frac{-q\emptyset_{bn}}{kT}\right) \quad (6)$$

where A and A^* denote the contact diode area and the effective Richardson constant, respectively. $\emptyset_{b_n}$ represents the effective barrier height.

From the saturation current Eq. (6), extract the BH and take the logarithm of both sides:

$$\ln(I_s) = \ln(AA^*T^2) + \left(\frac{-q\emptyset_{bn}}{kT}\right) \quad (7)$$

$$\ln(AA^*T^2) - \ln(I_s) = \left(\frac{q\emptyset_{bn}}{kT}\right) \quad (8)$$

Employing Is values, the zero bias barrier height $\emptyset bn$ values are obtained from the following relation:

$$\therefore \emptyset_{bn} = \frac{kT}{q}\ln\left(\frac{AA^*T^2}{I_s}\right) \quad (9)$$

It is commonly known that the theoretical connection between $\emptyset_{b_n}$ and $\emptyset_m$ is provided by:

$$\emptyset_{b_n} = \emptyset_m - \chi_{sc} \quad (10)$$

where χ_{sc} is the electronic affinity, ϕ_m is the work function of metals.

Then, the factor ideality n can be computed from the slope equation of the linear fit plot of the $lnI - V$ from the semi-log $lnI - V$. So:

$$\ln(I) = \frac{q}{nkT} + \ln(I_s) \quad (11)$$

By taking the derivative of Eq. (11), we can apply the following relation to extract n for each plot:

$$n = \frac{q}{kT}\frac{dV}{d\ln(I)} \quad (12)$$

Figure (4) displays the semi-logarithmic profiles of the $I - V$ curves of the n-AlGaAs heterojunction diode over a wide voltage range (±2V) at a specific temperature (100K – 500K). The profiles of ln I − V have been extracted from the I − V values at lower positive voltages, which exhibited good rectifying behavior. However, at high bias voltages, a deviation from the linearity curve occurs due to the effect of series resistances [29]. Additionally, it has been observed that as the temperature rises, the linear area shifts to lower voltage values. To identify the potential present transport system for our device, $\emptyset bn$, and Is parameters were computed for the zone where the modification of $lnI - V$ is linear. All these calculations were based on the Following Equation. (6), (9), and (12).

The results are presented in Figure 5 and summarized in Table 2. As noted in the TE theory, the n value is expected to be equivalent to unity in a perfect situation [30]. Nevertheless, an elevated value of n is obtained, which means a deviation from TE theory. These higher values of n at low temperatures may be due to the breadth of the depletion region (Wd) and levels formed by interface states, based on the density of doping atoms, as discussed in [30, 31]. Several other parameters, including non-ideal current flow, barrier inhomogeneity development, generation–recombination effects, series resistances, the spatial intensity distribution of Nss, and surface cleaning procedures, all influence the ideal factor for semiconductor diodes [32]. All of these elements have the potential to produce an ideality factor larger than 1 and deviate from the ideal behavior defined by the ideal diode equation [33].

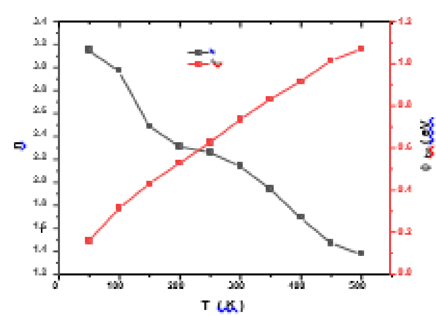

Fig. 5. Temperature dependance of n and $\emptyset bn$ values at a range of temperatures (50K-500K).

In reality, the barrier level has an indented shape and is not homogeneous, indicating that the energy levels are not uniform. If electrons do not have enough energy, they encounter obstacles that high energy levels cannot overcome. As a result, electrons with sufficient energy can easily cross the barrier when they come into contact with lower energy levels. This situation causes current values to increase even more [34]. As seen in Figure (5), the n value has a double Gaussian distribution and it decreases with increasing temperature, $\emptyset bn$ increases almost exponentially.

A linear association between n and $\emptyset bn$ was shown in the work by Schmitsdorf et al. [35], which was according to Tung's theoretical lateral inhomogeneities approach. Two distinct linear zones based on temperature are observed in the $\emptyset bn - n$ plot of the n-AlGaAs Schottky diode illustrated in Figure 6. By extrapolating the $\emptyset bn - n$ figure to = 1 , the homogeneous barrier height in the first area (50K –150 K) was found to be 0.55 eV.

In the high-temperature range (T > 150K), this value was found to be 1.05 eV. As the temperature drops, the primary current begins to vary from the ideal TE model, suggesting that lateral inhomogeneities are effective in the device [36, 37].

Narrowing the depletion zone width and certain physical conditions, like surface flaws, a high density of interfacial states, and non-homogeneous doping concentration, could produce these events. These observations are related to the non-pure TE current [38]. Because the charge carriers do not have enough energy to cross the high barrier height at a low temperature, current transport is possible in the lower parts of the BH [34]. This variation of ideality factors and barrier height values suggests that n-AlGaAs is not an ideal diode, and its charge transport mechanism is not just TE [33].

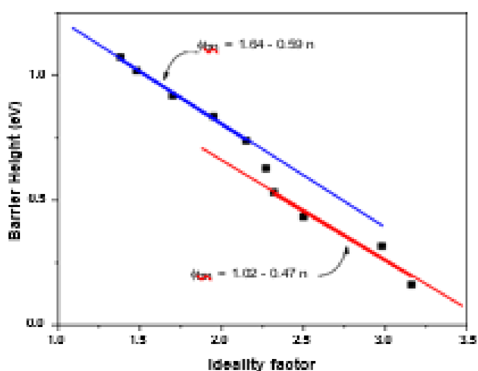

Fig. 6. $\emptyset bn$ *vs* plots of the n-AlGaAs Schottky diode.

3.2.2. Cheung- Cheung method`s

Then, all these parameters are extracted by an approach called the Cheung-Cheung function method. The Cheung-Cheung approach method [30, 39] used to obtain diode parameters from the $I - V$ characteristics in the forward bias using the following equation:

$$G(I) = \frac{\partial V}{\partial ln(I)} = R_s I + nV_t \quad (13)$$

$$H(I) = V - \frac{nkT}{k} \ln\left(\frac{I_s}{AA^*T^2}\right) \quad (14)$$

By combining Eq. (13) and Eq. (14), and after some steps (I) will be given as:

$$H(I) = R_s I + n\emptyset_{b_n} \quad (15)$$

where the RsI term represents the series resistance from above Eq. (13). As expected, the $dV/dl(I) - I$ trends in Figure 7 are linear. From Eq. (13) and Eq. (14), the Rs values were enumerated from the slopes of $dV/dl(I) - I$ curve drawn from Eq. (13), as shown in Figure 7. The n values were resolved from the y-axis intercept of the linear relation of $V/dln(I) - I$ plots.

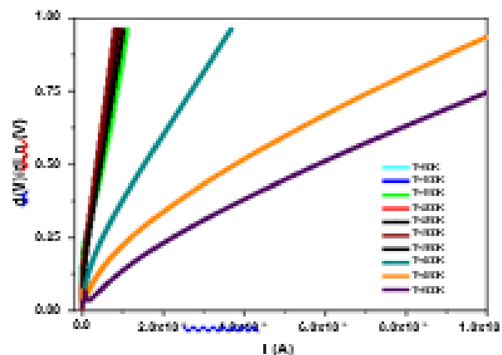

Fig. 7. The plots of $dV/dl(I)$ *vs* I for the n-AlGaAs SD at a range of temperatures (50K-500K).

Using the values of n determined from Eq. (13), they are substituted into Eq. (14) to obtain the $(I) - I$ plot. Figure 8 shows the plot of (I) *versus* I for the simulated diodes. This plot is a linear curve, where the y-axis intercept can be obtained from a slope of the (I) *versus* I plot. The evaluated parameters of the simulated diodes were determined using two methods: first, the linear region of the $dV/dl(I)$ *versus* I , and second, the $H(I)$ *versus* I plots, which are tabulated in Table 2. The n factor ideality vs temperature that the two models were able to obtain is displayed in Figure 9. This figure show that, for both models, n rises as the temperature decreases. At low temperatures, the TE field is responsible for the increases in n [40, 41]. Figure 10, illustrate how the $\emptyset bn$ values increase with temperature

in a comparable way for the TE and Cheung-Cheung techniques.

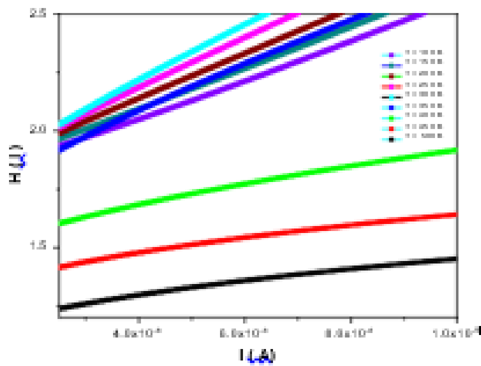

Fig. 8. (I) *versus* I plots of the n-AlGaAs Schottky diode.

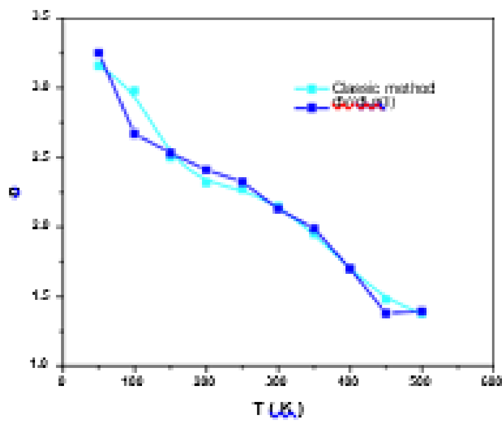

Fig. 9. Temperature dependence of the refractive indices n calculated by the Classic method and $dV/dl(I)$ curve.

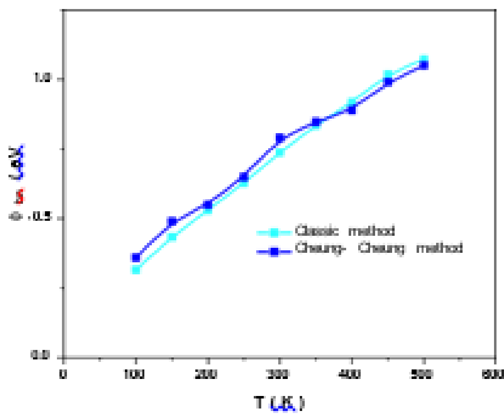

Fig. 10. Temperature dependence of the barrier height $\emptyset bn$ values calculated by the Classic and Cheung- Cheung methods.

Temperature also affects the series resistance, which usually rises with temperature. This can change the ideality factor, barrier height, and measured current, particularly at high temperatures. The $Rs - T$ graph is given in Figure 11 for the diode. The values of Rs obtained from $dV/dl(I) - I$ curve and $H(I) - I$ curves are suitable for one another.

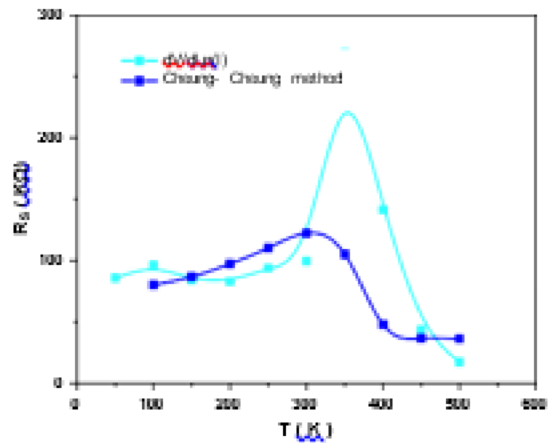

Fig. 11. R *ersus* T graph of the n-AlGaAs Schottky diode.

The results of the comparison between model fitting curves and experimental measurements are depicted in figure 12. These results are consistent with previously reported results, indicating that the diode is in good simulated if we compare it with the one fabricated.

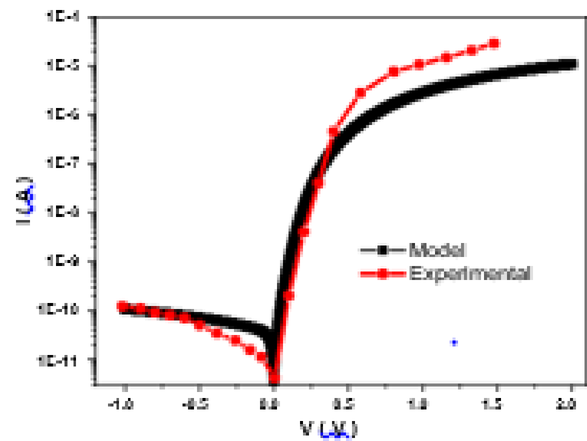

Fig. 12. Comparison between experimental and theoretical $I - V$ characteristics.

Journal of Manufacturing Engineering, September 2025, Vol. 20, Issue. 3, pp 113-121
DOI: https://doi.org/10.37255/jme.v20i3pp113-121

Table 1 - The values of the work Function of some Metals used in the simulation.

Metals	Work Function (eV)	Reference
Ag	4.64 4.26 4.3 4.70 4.32	[24] [21] [21] [24, 23]
Au	5.1 4.8	[24, 21] [21]
Cr	4.5 4.6 4.5	[21] [24, 21] [23]
Cu	4.94 4.4 4.65 4.70	[24] [21] [23] [24]
W	4.63 4.55	[24] [21, 23]
Co	5	[24, 23]
Re	4.96	[24, 23]

Table 2 - The electrical parameters, in a range of 50K to 500K temperatures, calculated using different methods.

T (K)	$lnI - V$			$\frac{dV}{dln(I)}$		$H(I) - I$	
	n	$\emptyset b_n (eV)$	$I_S (A)$	n	$R_S (K\Omega)$	$\emptyset b_n (eV)$	$R_S (K\Omega)$
50	3.16	0.162	$2.26\ 10^{-14}$	3.25	85.80		
100	2.98	0.316	$2.25\ 10^{-13}$	2.67	96.18	0.36	80.132
150	2.5	0.434	$1.15\ 10^{-11}$	2.53	84.18	0.49	86.814
200	2.32	0.531	$3.25\ 10^{-10}$	2.41	82.98	0.55	97.389
250	2.27	0.628	$2.55\ 10^{-9}$	2.33	93.83	0.65	110.34
300	2.15	0.738	$6.84\ 10^{-9}$	2.16	99.42	0.79	122.323
350	1.95	0.835	$2.25\ 10^{-9}$	1.99	114.32	0.848	105.084
400	1.7	0.918	$6.95\ 10^{-8}$	1.7	141.44	0.89	47.89
450	1.48	1.018	$1.55\ 10^{-7}$	1.38	43.73	0.99	36.68
500	1.38	1.073	$2.76\ 10^{-7}$	1.39	17.42	1.05	36.31

4. Conclusion

In the present work, n-AlGaAs Schottky diodes were successfully studied. The SBD's primary electronic characteristics were investigated utilizing the I-V simulated approach with varying values of Metal-Work Functions ($\emptyset m$) at room temperature. $I - V$ for different values of $\emptyset m$ show that the current and the threshold voltage increase with increasing $\emptyset\ m$. Current-voltage properties have been examined in the temperature range of 50 K to 500 K. The TE theory was used to calculate the ideality factor (n) and $\emptyset bn$ values at various temperatures. It is significant to observe that, in contrast to the $\emptyset bn$ value, the n value diminishes with rising temperatures. The Chung-Chung method has also been used to calculate these parameters, including the Rs value. In addition, TE theory and the Chung-Chung method have shown that the $\emptyset bn$ values increase with temperature, in contrast to the effect of n. Consequently,

 © SME

it was shown that the fundamental parameters (n, $\emptyset bn$, Rs), were significantly affected by temperature. Therefore, higher n values were observed due to the inhomogeneity of the barrier and generation-recombination. Therefore, we can conclude that these outcomes in the parameters (n, $\emptyset bn$, and Rs), which determine the SD's performance based on voltage and temperature, demonstrate the device's suitability for use in electrical and optoelectronic applications.

References

1. *L. Łukasiak, and A. Jakubowski, History of Semiconductors, "Journal of Telecommunications and Information Technology", vol. 1, pp. 3–9, 2010.*

2. *N. Mesai, I. Lemkadem, and A. Benaouda, "Étude de l'effet de température sur la diode Schottky," 2020.*

3. *N. K. R. Nallabala, S. V. Prabhakar, V. Verma, R. Singh, S. Alhammdi, V. Krishaiah, K. Manjunath, V. M. Dhanalakshmi, and V. R. Minnam Reddy, "Highly sensitive and cost-effective metal-semiconductor-metal asymmetric type Schottky metallization based ultraviolet photodetecting sensors fabricated on n-type GaN," *Materials Science in Semiconductor Processing*, vol. 138, 106297, 2022.*

4. *M. Ulusoy, Y. Badali, G. Pirgholi-Givi, Y. Azizian-Kalandaragh, and S. Altındal, "The capacitance/conductance and surface state intensity characteristics of the Schottky structures with ruthenium dioxide-doped organic polymer interface," *Synthetic Metals*, vol. 292, 117243, 2023.*

5. *Kocyigit, M. Yilmaz, S. Aydogan, Ü. İncekara, and H. Kacus, "Comparison of n- and p-type Si-based Schottky photodiodes with interlayered Congo red dye," *Materials Science in Semiconductor Processing*, vol. 135, 106045, 2021.*

6. *N. Sghaier, S. Bouzgarrou, M. M. Ben Salem, A. Souifi, A. Kalboussi, and G. Guillot, "I–V anomalies on InAlAs/InGaAs/InP HFETs and deep levels investigations," *Materials Science and Engineering B*, vol. 121, pp. 178–182, 2005.*

7. *S. Bouzgarrou, M. M. Ben Salem, F. Hassen, A. Kalboussi, and A. Souifi, "DLTS and PL study of defects in InAlAs/InP heterojunctions grown by metal organic chemical vapor deposition," *Materials Science and Engineering B*, vol. 116, pp. 202–207, 2005.*

8. *M. M. Ben Salem, S. Bouzgarrou, N. Sghaier, A. Kalboussi, and A. Souifi, "Correlation between static characteristics and deep levels in InAlAs/InGaAs/InP HEMTs," *Materials Science and Engineering B*, vol. 127, no. 1, pp. 34–40, 2006.*

9. *S. Bouzgarrou, N. Sghaier, M. M. Ben Salem, A. Souifi, and A. Kalboussi, "Influence of interface states and deep levels on output characteristics of InAlAs/InGaAs/InP HEMTs," *Materials Science and Engineering C*, vol. 28, pp. 676–679, 2008.*

10. *S. Bouzgarrou, M. M. Ben Salem, A. Kalboussi, and A. Souifi, "Experimental and theoretical study of parasitic effects in InAlAs/InGaAs/InP HEMTs," *American Journal of Physics and Applications*, vol. 1, no. 1, pp. 18–24, 2013, doi: 10.11648/j.ajpa.20130101.14.*

11. *Türüt, "On current-voltage and capacitance-voltage characteristics of metal-semiconductor contacts," *Turkish Journal of Physics*, vol. 44, pp. 302–347, 2020.*

12. *F. Acar, A. Buyukbas-Ulusan, and A. Tataroglu, "Analysis of interface states in Au/ZnO/p-InP (MOS) structure," pp. 1–8, 2018.*

13. *Sadoun and I. Kemerchou, "Extraction of the electrical parameters of the Au/InSb/InP Schottky diode in the temperature range (300 K–425 K)," *International Journal of Energetica (IJECA)*, vol. 5, no. 1, pp. 2543–3717, 2020.*

14. *S. Demirezen, A. Arslan Alsac, H. G. Çetinkaya, and S. Altındal, "The investigation of current-transport mechanisms (CTMs) in the Al/(In2S3:PVA)/p-Si (MPS)-type Schottky barrier diodes (SBDs) at low and intermediate temperatures," *Journal of Materials Science: Materials in Electronics*, vol. 34, p. 1186, 2023.*

15. *Buyukbas-Ulusan, A. Tataroglu, and S. Altındal-Yerişkin, "Analysis of the current transport characteristics in Au/n-Si Schottky diodes with Al2O3 interfacial layer over wide temperature range," *ECS Journal of Solid-State Science and Technology*.*

16. *N. A. Al-Ahmadi, "Metal oxide semiconductor-based Schottky diodes: A review of recent advances," *Materials Research Express*, vol. 7, 032001, 2020.*

17. *D. Caughey and R. Thomas, "Carrier mobilities in silicon empirically related to doping and field," *Proceedings of the IEEE*, vol. 55, pp. 2192–2193, 1967.*

18. *S. Selberherr, "Process and device modeling for VLSI," *Microelectronics Reliability*, vol. 24, pp. 225–257, 1984.*

19. *S. Selberherr, *Analysis and Simulation of Semiconductor Devices*. Springer Science & Business Media, 2012.*

20. *W. Shockley and W. T. Read Jr., "Statistics of the recombinations of holes and electrons," *Physical Review*, vol. 87, pp. 835–842, 1952.*

21. *M. Stössel, J. Staudigel, F. Steuber, J. Simmerer, and A. Winnacker, "Impact of the cathode metal work function on the performance of vacuum-deposited organic light emitting devices," *Applied Physics A*, vol. 68, pp. 387–390, 1999.*

22. *Ghods, "Design and fabrication of field-effect III–V Schottky junction solar cells," 2020.*

23. *H. Helal, Z. Benamara, M. Ben Arbia, A. Rabehi, A. C. Chaouche, and H. Maaref, "Electrical behavior of n-GaAs based Schottky diode for different contacts: Temperature dependence of current voltage," *International Journal of Numerical Modelling*, vol. 34, e2916, 2021.*

24. *H. Helal, Z. Benamara, A. H. Kacha, M. Amrani, A. Rabehi, B. Akkal, G. Monier, and C. Robert-Goumet, "Comparative study of ionic bombardment and heat treatment on the electrical behavior of Au/GaN/n-GaAs Schottky diodes,"*

Superlattices and Microstructures, vol. 135, 106276, 2019.

25. H. Altan, M. Özer, and H. Ezgin, "Investigation of electrical parameters of Au/P3HT:PCBM/n-6H–SiC/Ag Schottky barrier diode with different current conduction models," *Superlattices and Microstructures*, vol. 146, 106658, 2020.

26. Kumar, A. Kumar, K. K. Sharma, and S. Chand, "Analysis of anomalous transport mechanism across the interface of Ag/p-Si Schottky diode in wide temperature range," *Superlattices and Microstructures*, vol. 128, pp. 373–381, 2019.

27. D. K. Schroder, *Semiconductor Material and Device Characterization*, 2006.

28. Barkhordari, S. Ozçelik, G. Pirgholi-Givi, H. R. Mashayekhi, S. Altındal, and Y. Azizian-Kalandaragh, "Dielectric properties of PVP:BaTiO3 interlayer in the Al/PVP:BaTiO3/p-Si structure," *Silicon*, vol. 14, no. 10, pp. 5437–5443, 2022.

29. P. R. S. Reddy, V. Janardhanam, K.-H. Shim, V. R. Reddy, S. N. Lee, S.-J. Park, and C.-J. Choi, *Vacuum*, vol. 171, 109012, 2020.

30. Barkhordari, H. R. Mashayekhi, P. Amiri, S. Altındal, and Y. Azizian-Kalandaragh, "Optoelectric response of Schottky photodiode with a PVP:ZnTiO3 nanocomposite as an interfacial layer," *Optical Materials*, vol. 148, 114787, 2024.

31. M. Nawar, M. Abd-Elsalam, A. M. El-Mahalawy, and M. M. El-Nahass, "Analyzed electrical performance and induced interface passivation of fabricated Al/NTCDA/p-Si MIS–Schottky heterojunction," *Applied Physics A*, vol. 126, 113, 2020.

32. O. Çiçek, H. U. Tecimer, S. O. Tan, H. Tecimer, S. Altındal, and I. Uslu, "Evaluation of electrical and photovoltaic behaviors of Au/n-GaAs diodes with and without pure and graphene-doped PVA interfacial layers under dark and illuminated conditions," *Composites Part B*, vol. 98, pp. 260–268, 2016.

33. S. M. Sze, *Physics of Semiconductor Devices*, 2nd ed., Wiley, New York, 1981.

34. Q. Zhou, H. Wu, and H. Li, "Barrier inhomogeneity of Schottky diode on nonpolar AlN grown by physical vapor transport," *IEEE Journal of the Electron Devices Society*, vol. 7, pp. 662–667, 2019.

35. H. Elamen, Y. Badali, M. Ulusoy, Y. Azizian-Kalandaragh, S. Altındal, and M. T. Güneşer, "The photoresponse behavior of a Schottky structure with a transition metal oxide-doped organic polymer (RuO2:PVC) interface," *Polymer Bulletin*, vol. 81, pp. 403–422, 2024.

36. S. Altındal, O. A. Faruk, S. Özdemir, A. Aydogan, and A. Türüt, "Discrepancies in barrier heights obtained from current–voltage and capacitance–voltage of Au/PNoMPhPPy/n-GaAs structures in wide range of temperature," *Journal of Materials Science: Materials in Electronics*, vol. 33, pp. 12210–12223, 2022.

37. Y. Badali, H. Altan, and S. Altındal, "Thermal dependence on electrical characteristics of Au/(PVC:Sm2O3)/n-Si structure," *Journal of Materials Science: Materials in Electronics*, vol. 35, p. 228, 2024.

38. R. Deniz, A. I. Tas, Z. Çaldıran, Ü. Incekara, M. Biber, S. Aydogan, and A. Türüt, "Effects of PEDOT:PSS and crystal violet interface layers on current-voltage performance of Schottky barrier diodes as a function of temperature and variation of diode capacitance with frequency," *Current Applied Physics*, vol. 39, pp. 173–182, 2022.

39. R. Deniz, "The temperature dependence of current–voltage characteristics of V2O5/p-Si heterojunction diode," *Journal of Materials Science: Materials in Electronics*, vol. 32, pp. 18886–18899, 2021.

40. İ. Taşçıoğlu, G. Pirgholi-Givi, S. Altındal Yerişkin, and Y. Azizian-Kalandaragh, "Examination on the current conduction mechanisms of Au/n-Si diodes with ZnO–PVP and ZnO/Ag2WO4–PVP interfacial layers," *Journal of Sol-Gel Science and Technology*, vol. 107, pp. 536–547, 2023.

41. J. O. Bodunrin and S. J. Moloi, "Current-voltage characteristics of 4 MeV proton-irradiated silicon diodes at room temperature," *Silicon*, vol. 14, pp. 10237–10244, 2022.